ELSEVIER

Physica B 319 (2002) 78–89

PHYSICA B

www.elsevier.com/locate/physb

Crystal-field interactions and magnetism in rare-earth transition-metal intermetallic compounds

R.J. Radwanski[a,b,*], R. Michalski[a,b], Z. Ropka[a], A. Blaut[a]

[a] *Center of Solid State Physics, S^{nt} Filip 5, 31-150 Krakow, Poland*
[b] *Institute of Physics, Pedagogical University, 30-084 Krakow, Poland*

Received 6 March 2002; received in revised form 13 March 2002

Abstract

The description of basic experiments of the rare-earth hard magnetic materials, high-field magnetization curves on single-crystalline samples of Ho_2Co_{17} and $Nd_2Fe_{14}B$ is reviewed with the aim to derive parameters physically relevant on atomic scale. The anisotropic magnetic properties have been found to be of single-ion origin. The successful description of the rare-earth compounds Ho_2Co_{17}, $Nd_2Fe_{14}B$, $Pr_2Fe_{14}B$, $ErNi_5$, $PrRu_2Si_2$, $ErRu_2Si_2$ in terms of the crystal-field, spin–orbit and inter-site magnetic interactions proves the existence, in a solid, the discrete atomic-like low-energy electron structure that predominantly governs the magnetic and electronic properties. The macroscopic properties have been correlated with the atomic-scale parameters. These studies reveal the importance of the low-symmetry crystal-field interactions (high-order charge multipolar interactions) in description of the magnetic properties of 4f compounds.

Keywords: Crystalline-electric field; Magnetism; Spin–orbit coupling; Transition metals; Hund rules; Ho_2Co_{17}; $Nd_2Fe_{14}B$; $Pr_2Fe_{14}B$; $ErNi_5$; $PrRu_2Si_2$; $ErRu_2Si_2$

1. Introduction

The aim of this paper is to present a consistent understanding of the electronic and magnetic properties of the transition-metal compounds, Ho_2Co_{17}, $Nd_2Fe_{14}B$, $ErNi_5$, $PrRu_2Si_2$ and $ErRu_2Si_2$. All of them are intermetallics. They belong to a very large class of 3d–4f compounds that is important from both theoretical and applicational point of view [1]. Successful studies on these compounds have been possible mainly thanks to two factors: the availability of large single crystals and modern experimental techniques, like for instance magnetic measurements in high magnetic fields, low-temperature specific heat and inelastic neutron scattering.

These studies allow for the determination of basic interactions like the strength of the 3d–4f interaction and of the crystal-field interactions that govern their magnetic and electronic properties.

*Corresponding author. Center of Solid State Physics, S^{nt} Filip 5, 31-150 Krakow, Poland. Tel.: +48-12-633-61-46; fax: +48-12-632-40-12.

E-mail address: sfradwan@cyf-kr.edu.pl (R.J. Radwanski).
URL: http://www.css-physics.edu.pl.

2. Ho_2Co_{17}—first-order moment reorientation

The magnetization curves of the single-crystalline Ho_2Co_{17}, measured up to 35 T along three

0921-4526/02/$ - see front matter
PII: S0921-4526(02)01110-9

main crystallographic directions (Fig. 1) [2,3], have revealed (i) very anisotropic behavior with the magnetic moments in the hexagonal plane, the hard hexagonal *c*-axis and the easy magnetization direction (EMD) along the *b*-axis, (ii) a metamagnetic transition at 22 T for fields applied along the easy *b* direction, and (iii) a metamagnetic transition at 29 T for fields applied along the *a* direction. For the interpretation of this anisotropic behavior and of the metamagnetic transition, we have employed a model [4], called the two-sublattice model below. According to this model all 3d moments form one magnetic sublattice described by the resultant magnetization M_T and the magnetocrystalline anisotropy (MCA) energy E_a^T. All rare-earth (R) moments form the second magnetic sublattice described by the resultant magnetization M_R and the MCA energy E_a^R. The

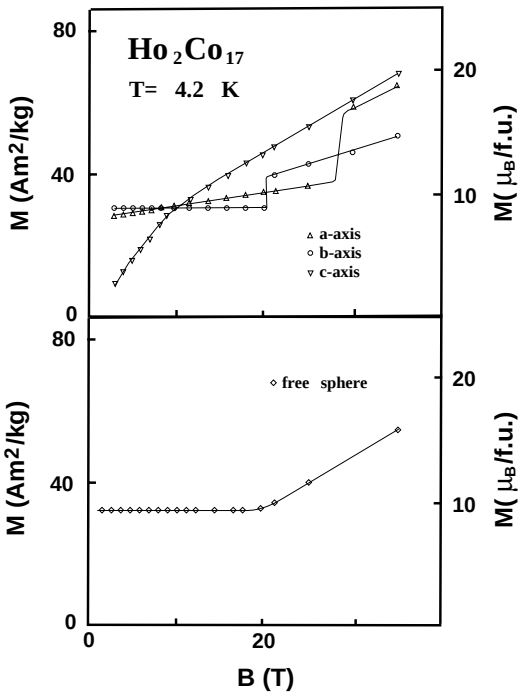

Fig. 1. Magnetization curves of single-crystalline Ho_2Co_{17}, measured along three main hexagonal crystallographic directions [2] and high-field magnetization curves, measured on the free-to-rotate single-crystalline sphere of Ho_2Co_{17} (practically the same curve is obtained on a sample consisting of free powder particles) [3].

experimental value of the easy-axis magnetization M_s of Ho_2Co_{17} of 33.6 Am^2/kg, corresponding to 8.0μ_B/f.u., yields $M_T = 28\mu_B$/f.u. if one assumes the full Ho moment of 10μ_B/Ho-ion and $M_R = 20\mu_B$/f.u. and antiparallel moment alignment [3,5]. Attributing 28.0μ_B/f.u. to the Co-sublattice magnetization is very plausible as it corresponds to 1.65μ_B/Co-atom, which is only slightly smaller than the Co-metal moment. According to the two-sublattice model, the special magnetization behavior can be attributed to the rare-earth sublattice, to the special angular shape of the MCA energy E_a^T. The value and the angular dependence of E_a^T was taken quite normal like observed in Y_2Co_{17}, i.e. −11 K/f.u. The Co magnetization prefers to stay within the hexagonal plane, but relatively weakly. The Co anisotropy field amounts to 1.2 T only.

In the two-sublattice model, for describing the high-field magnetization process, we have used the energy expression

$$E_{R-T} = E_a + E_{exch} + E_M. \quad (1)$$

This expression contains terms with the magnetocrystalline anisotropies E_a, the exchange energy E_{exch} between the two magnetic sublattices and the magnetostatic energies E_M due to the external magnetic field. This energy expression becomes quite simple if we assume that, during the magnetization process, both magnetizations rotate only within the hexagonal plane (this assumption means that the out-plane anisotropy energy is much larger than the in-plane anisotropy, which is reasonable). For an external field B applied along the easy *b*-axis, Eq. (1) takes the form [4,6–8]

$$\begin{aligned} E_{R-T} = & -M_R B\cos a - M_T B\cos\beta \\ & + K_4^R\cos 6\alpha + K_4^T\cos 6\beta \\ & + n_{RT} M_R M_T \cos(\alpha+\beta), \end{aligned} \quad (2)$$

where α and β denote azimuthal angles of two sublattice magnetizations with respect to the magnetic field direction. At zero field $\alpha = 180^\circ$ and $\beta = 0^\circ$. K_4^R and K_4^T denote the in-plane anisotropy constants. For the given values of M_T and M_R, the transition field depends critically on the R–T intersublattice coupling n_{RT} and the K_4^R value (we took $K_4^T = 0$). The full magnetization

curve, calculated for fields applied along the easy direction, is shown in Fig. 2. The calculated curve exhibits three sharp magnetic transitions—according to the presented interpretation they are related to the sharp rotation of the Ho-sublattice magnetization, with the increasing magnetic field, to the next easy direction within the hexagonal plane. The final situation is the forced ferromagnetic state reached in large external fields. Similar transitions occur in the magnetization along the hard axis in plane, the *a*-axis in case of Ho_2Co_{17}. We have named these transitions first-order moment reorientation (FOMR) transitions. The general shape of the magnetization curve of Fig. 2 can be understood as a continuous increase of the magnetization due to the bending of the antiparallelly aligned moments with transitions governed by the in-plane anisotropy. The calculations have predicted the occurrence of other transitions for the *b* direction at 45 and 102 T. The transition at 44 T has been detected 14 years after its prediction in measurements at Osaka High-Field Laboratory in 1991 [9].

Having the experimental value of the transition field, we have derived a n_{RT} value of 0.55 T kg/Am^2. The physical visualization of this n_{RT} value is the molecular field B^R_{mol} ($=n_{RT}\cdot M_T$). B^R_{mol} is

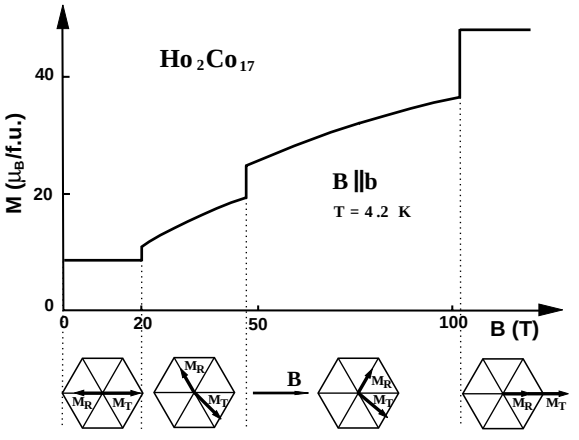

Fig. 2. Calculated magnetization curve of Ho_2Co_{17} for external fields applied along the EMD (*b*-axis). The three transitions are due to jump of the Ho-sublattice magnetization to the next easy direction within hexagonal plane closer to the applied-field direction.

experienced by the Ho moment in Ho_2Co_{17} but it is produced by the Co sublattice. The derived value of n_{RT} yields B^{Ho}_{mol} of 64 T.

The shown interpretation has enabled the first physically adequate evaluation of the strength of the 3d–4f coupling. Earlier estimations of the molecular field were 3–5 times larger. On this basis, serious objections have arisen against our interpretation and the against the possibility of the formation of a non-collinear magnetic structure already in an external field of 20 T. If the molecular field and 3d–4f interactions were much stronger, the external field would not be able to disturb the internal magnetic structure. The physical correctness of our model was confirmed shortly after—the FOMR transition has been detected in Dy_2Co_{17} at 28 T [10] in agreement with our earlier predictions [6,7]. The FOMR transitions in the tetragonal plane were also detected in the compound $Er_2Fe_{14}B$ [11].

3. Ho_2Co_{17}—hard axis magnetization curve

The full energy expression given by Eq. (1) for the coupled two R- and T-sublattice magnetizations in an external field B_0 takes the form

$$E_{R-T} = E^R_a + E^T_a + n_{RT} M_T M_R - M_T \cdot B_0 - M_R \cdot B_0. \quad (3)$$

For the anisotropy energy we made use of an expression with the Legendre functions with the anisotropy coefficients κ^m_n:

$$E_a(\theta,\varphi) = \sum\sum \kappa^m_n P^m_n(\cos\theta)\cos m\varphi, \quad (4)$$

instead of the customarily used expansion in terms of the sinus, with the anisotropy constants K^m_n. The Legendre-function expansion later enables one to correlate the magneto-crystalline energy with the CEF interactions. The relations between K^m_n and κ^m_n are found in Ref. [1, p. 484].

The bending of two sublattice magnetizations under the action of the external magnetic fields is evident if we note that the hard-axis magnetization exceeds that measured along the nominally easy axis, above 12 T in case of Ho_2Co_{17}. This observation reveals that the apparent anisotropy field B_A of 12 T, that one may derive from

low-field measurements, does not have the physical meaning of an anisotropy field. This effect was discussed in much detail for $Dy_2Fe_{14}B$, where the hard-axis magnetization crosses the easy-axis magnetization at 22 T and is 1.4 times larger at a field of 35 T [12]. In fact, the apparent anisotropy field, the crossing of hard and easy-magnetization curves is a measure of the n_{RT} parameter rather than of the anisotropy energy. This becomes clear from the analysis of the magnetization process of anisotropic ferrimagnets in high magnetic fields. The full high-field magnetization curves on $GdCo_5$, Gd_2Co_{17}, Gd_2Co_7 and $GdCo_3$, as examples, have been calculated up to field of 400 T, where the forced ferromagnetic state is realized [13]. These theoretical predictions about the high-field magnetization process have been confirmed by experiments on $GdCo_5$ and Gd_2Co_7 [14,15].

It is worth noting that the parameter n_{RT} derived from the above analysis of the easy- and hard-axis magnetization curves of Ho_2Co_{17} is practically the same—thus our studies do not give any indication for anisotropic exchange.

4. 3d–4f coupling

In a systematic study of the FOMR transitions in Ho_2Co_{17} and Dy_2Co_{17}, and later in Ho_2Fe_{17}, $Ho_2Co_{14}Fe_3$, we got confirmation about the strength of the 3d–4f coupling. Assuming that the coupling mechanism between the rare-earth and Co moments proceeds via the rare-earth spin rather than via the total moment, we could transform the value of the n_{RT} coefficient from one compound to another compound, with the same composition, i.e. from Ho_2Co_{17} to Dy_2Co_{17} and to Ho_2Fe_{17}, for instance. If the spin moment is involved in the coupling, the spin field B_S^R, acting on the R-spin moment, plays a more fundamental role than the molecular field B_{mol}^R.

The spin and the molecular fields are interrelated by

$$B_S^R = \frac{g_L}{2(g_L - 1)} B_{mol}^R, \tag{5}$$

where g_L is the Landé factor of the R-atom involved. In the R_2Co_{17} series, B_S^R amounts to 164 T.

In order to transform the n_{RT} coefficient from one compound to another with a different composition, we develop the microscopic model for the 3d–4f coupling between the 3d and 4f magnetization sublattices as originating from the Heisenberg-like Hamiltonian between the 3d and 4f spins, S_T and S_R. Then, the number of Co nearest neighbors z surrounding a Ho atom appears and we come to an expression for B_S^R as:

$$B_S^R = \frac{A_{RT} S_T z}{\mu_B}, \tag{6}$$

where A_{RT} is the microscopic Heisenberg-like 3d–4f coupling parameter. The experimental value of 64 T for B_{mol}^R in Ho_2Co_{17} yields A_{RT} of -6.7 K (the negative sign denotes the antiferromagnetic coupling). Values for B_{mol}^R and B_S^R for rare-earth Co compounds R_nCo_m, based on this value of the A_{RT} parameter, have been presented in Ref. [16], and for rare-earth compounds with iron R_nFe_m in Ref. [17].

The evaluation of the 3d–4f coupling from the magnetization curves is very accurate for compounds with antiparallel alignment of two sublattice magnetizations, i.e. for heavy-rare-earth compounds. For light-rare-earth compounds with the parallel alignment, the applied strong field causes a non-coherent rotation of two magnetizations, but the determination of the n_{RT} parameter has a rather large error. Here, neutron studies turn out to be very useful. Apart from the spin dynamics, localized energy excitations can be detected. A localized excitation in Dy_2Co_{17} at 8.8 meV [18] and one in Nd_2Co_{17} at 16.5 meV [19] have been found in inelastic-neutron-scattering (INS) experiments. Attributing them to CEF excitations between the subsequent CEF states, a molecular field B_{mol}^R of 110 T in Dy_2Co_{17} and one of 320 T in Nd_2Co_{17} have been derived.

The combined high-magnetic-field studies and neutron studies allowed for evaluation of the 3d–4f coupling in all series of rare-earth-3d compounds. The derived values of the spin field are collected in Fig. 3. The spin field largely increases for light rare earths pointing to a much stronger 3d–4f coupling at the beginning of rare-earth series [20].

The 3d–4f coupling has been later studied very successfully by Verhoef on free-to-rotate

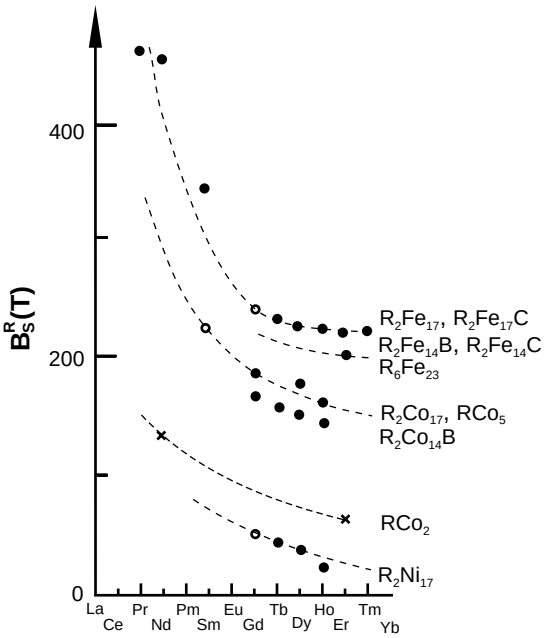

Fig. 3. Variation of the spin field B_S^R across the lanthanide series. The spin field B_S^R originates from the 3d-sublattice magnetization and acts on the R spin moment [20].

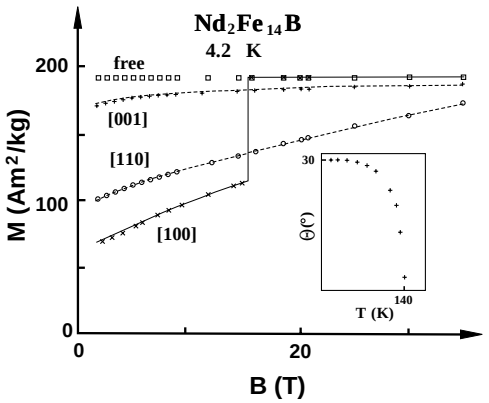

Fig. 4. Magnetization curves for single-crystalline $Nd_2Fe_{14}B$, measured along the three main tetragonal crystallographic directions [26]. The inset shows the tilting angle of the EMD with respect to the tetragonal c-axis.

single-crystals that could freely rotate in the field, yielding, because of their simplicity, very beautiful curves like the one shown in Fig. 1b, and by De Boer and co-workers on free-powder samples of practically all systems of known ferrimagnetic rare-earth—transition-metal intermetallic compounds [21–23].

5. $Nd_2Fe_{14}B$—importance of higher-order CEF interactions

In the late autumn of 1983, the compound $Nd_2Fe_{14}B$ with its very promising properties for the application as permanent magnet was discovered [24]. Due to its extraordinary magnetic properties, like uniaxial magnetic anisotropy, magnetic-ordering temperature well above—room temperature and consisting mostly of iron, not from expensive cobalt, $Nd_2Fe_{14}B$ soon got the name of supermagnet. Magnetic measurements on the single crystal $Nd_2Fe_{14}B$ revealed a wealth of quite unusual magnetic behavior, see Fig. 4 [25,26]. From the magnetization curves it was clear that the easy axis direction does not lie along any main crystallographic direction. The origin of the conical structure, with an easy direction that makes an angle of 30° with the tetragonal c-axis, was quite mysterious. It was fortunate for the application at room temperature that this conical structure disappears at 140 K. The description of the complex magnetic behavior of $Nd_2Fe_{14}B$ has been a real challenge for the whole magnetic community in the years 1985–1990, together with the subject of heavy fermions and the high-T_c superconductivity after its discovery in 1986.

We have applied the two-sublattice model assuming that the magnetic-moment value of Nd and Fe atoms is not affected by external fields, even as large as 35 T, and that all peculiarities of the magnetization curves are due to the formation of complex non-collinear magnetic structures, both in the presence of an external magnetic field as well as in zero field. The expansion of the anisotropy energy of the Nd-sublattice magnetization in terms of the Legendre functions turns out to be very useful as it enables one to judge the meaningfulness of the fitted values. Later, this expansion enabled us to correlate anisotropy coefficients κ_n^m to the atomic CEF parameters [27]. The angular shape of the total MCA energy of the Nd-sublattice E_a^{Nd}, derived from the

magnetization curves up to 40 T on a single crystal, is shown in Fig. 5 together with contributions from different multipolar terms. The unusual conical structure results from the significance of higher-order anisotropy terms, in particular of κ_4^0 and κ_6^4. Although, the general angular shape of E_a^{Nd} is largely governed by κ_2^0, the higher-order terms produce a minimum of the anisotropy energy at $\Theta = 30^\circ$. The metamagnetic transition along the

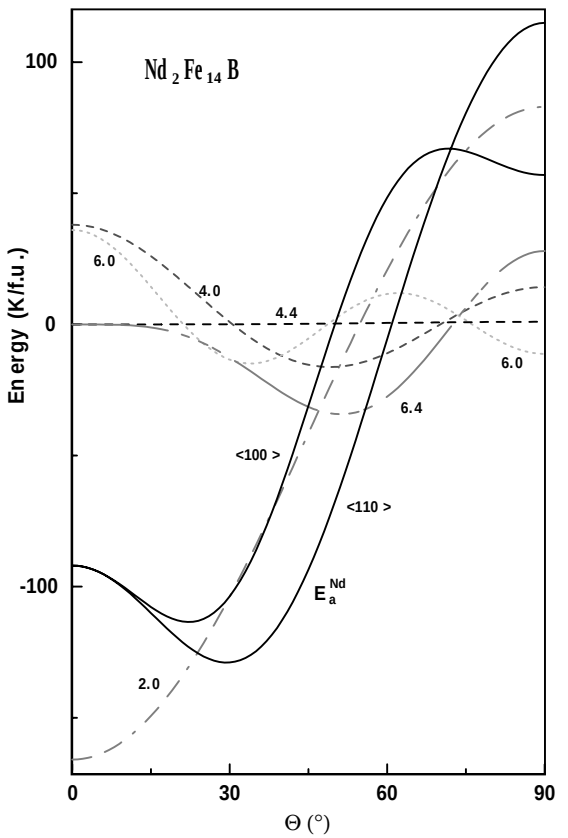

Fig. 5. Angular dependence of the MCA energy of the Nd-sublattice magnetization, derived from the magnetization curves shown in Fig. 3 for a single crystal in magnetic fields up to 40 T, in the planes $\langle 1\,1\,0 \rangle$ (bottom) and $\langle 1\,0\,0 \rangle$ (upper). The different multipole contributions $\kappa_n^m P_n^m(\cos\Theta)$ to the MCA energy are shown. The curves are labelled by values for (n, m). The conical structure of $Nd_2Fe_{14}B$ with EMD being tilted 30° from the tetragonal c-axis is due to the energy minimum in the $\langle 1\,1\,0 \rangle$ direction; the transition at 17 T is due to the energy minimum at 90° for the $\langle 1\,0\,0 \rangle$ direction. The difference in the energy curves for the $\langle 1\,1\,0 \rangle$ and $\langle 1\,0\,0 \rangle$ directions is due to the opposite sign of the in-plane anisotropy coefficients κ_4^4 and κ_6^4.

$\langle 1\,0\,0 \rangle$ axis is also due to these higher-order anisotropy contributions. They produce a minimum of the energy for this direction at $\Theta = 90^\circ$. Thanks to this, the magnetization can jump during the magnetization process to this energy minimum in an abrupt transition, at 16 T in the case of $Nd_2Fe_{14}B$, passing the maximum of the anisotropy energy. The found anisotropy coefficients $\kappa_2^0 = -166$ K/f.u., $\kappa_4^0 = +38$ K/f.u., $\kappa_6^0 = +36$ K/f.u., $\kappa_4^4 = -1$ K/f.u. and $\kappa_6^4 = +28$ K/f.u. yield the tetragonal CEF parameters, $B_2^0 = -2.36$ K, $B_4^0 = +13.5$ mK, $B_4^4 = -3.3$ mK, $B_6^0 = +1.66$ mK and $B_6^4 = +6.9$ mK. The anisotropy coefficients are related to the crystal-field parameters by the relation (Ref. [1, p. 329]):

$$\kappa_n^m = B_m^m \langle \hat{O}_n^m \rangle, \tag{7}$$

where the $\langle \hat{O}_n^m \rangle$ is the expectation value of the Stevens operators for $J_z = J$.

A quite similar analysis has been performed for $Pr_2Fe_{14}B$, that exhibits metamagnetic transitions at 13.2 and at 17.1 T in fields applied along the $\langle 1\,0\,0 \rangle$ and $\langle 1\,1\,0 \rangle$ axis, respectively [28,29]. Despite of the different rare-earth atoms we obtained a very successful description within the two-sublattice model with CEF coefficients close to those derived for $Nd_2Fe_{14}B$ [29,30]. The excellent description of such complex magnetization curves proves the high physical adequacy of the two-sublattice model and the CEF single-ion origin of the rare-earth MCA, despite of their metallic behavior. The discovered importance of the CEF interactions in rare-earth intermetallics has led us to study $ErNi_5$ and other compounds of this family.

6. $ErNi_5$

$ErNi_5$ has been studied as an examplary compound in which the CEF interactions can be thoroughly analyzed as the 3d–4f exchange is relatively weak. It crystallizes in the hexagonal structure and large single-crystalline samples can be grown as known from earlier work of the Grenoble group of Lemaire and Givord. $ErNi_5$ orders ferromagnetically below $T_c = 9$ K with moments along the hexagonal axis. The magnetic

ordering is seen in the temperature dependence of the specific heat as a large λ anomaly [31], see Fig. 6. The experimentally observed ordered Er magnetic moment m_{Er} equals $8.5\mu_{\mathrm{B}}$ [32,33]. We have attributed the special behavior of $ErNi_5$, compared to $LaNi_5$, to the presence of the Er^{3+} ions possessing the configuration $4f^{11}$. The associated electronic structure has been obtained by taking into account crystal-field (CEF) and inter-site spin-dependent interactions. The considered Hamiltonian contains single-ion-like (H_{f}) and inter-site ($H_{\mathrm{f-f}}$) terms [31]:

$$\begin{aligned} H &= H_{\mathrm{f}} + H_{\mathrm{f-f}} \\ &= \sum_n \sum_m B_n^m \hat{O}_n^m(J, J_z) \\ &\quad + n_{\mathrm{RR}} g_{\mathrm{L}}^2 \mu_{\mathrm{B}}^2 (-J\langle J\rangle + \tfrac{1}{2}\langle J\rangle^2) \\ &\quad + g_{\mathrm{L}}\mu_{\mathrm{B}} J \cdot B_{\mathrm{ext}}. \end{aligned} \tag{8}$$

The first term is the CEF Hamiltonian written for the lowest multiplet ($^4I_{15/2}$, $g_J = 6/5$). The second term represents the spin-dependent interactions between the Er moments written in the dynamical-mean-field approximation with the molecular-field coefficient n_{RR}. The last term describes the Zeeman effect and it allows to study the magnetic susceptibility in the paramagnetic region, for instance. g_{L} is the Landé factor for the lowest multiplet and the magnetic moment of the Er ion is expressed as $m_{\mathrm{R}} = -g_{\mathrm{L}} J \mu_{\mathrm{B}}$.

The energy level scheme of the $4f^{11}$ (Er^{3+} ion) in the crystal field of the hexagonal symmetry contains eight Kramers doublets, see Fig. 7. The Kramers degeneracy is removed by the internal molecular field. The internal molecular field $B_{\mathrm{mol}}^{\mathrm{Er}}$ equals $n_{\mathrm{RR}} \cdot m_{\mathrm{R}}$. This field has been calculated to be 1.5 T at 0 K for $ErNi_5$. A field of 350 T, for example, has been evaluated by us in $Nd_2Fe_{14}B$. $Nd_2Fe_{14}B$ exhibits, however, a T_{C} of about 500 K. Inspecting the experimental results for $ErNi_5$ presented in Fig. 6, one finds a very good theoretical description of the temperature dependence of the specific heat $c(T)$, including the λ type of peak at 9 K. Our calculations give a zero-temperature magnetic-moment value of $8.5\mu_{\mathrm{B}}$ and predict its direction along the hexagonal axis. The calculations provide also the anisotropy of the magnetic properties and the temperature dependence of the paramagnetic susceptibility in very good agreement with experimental data [31].

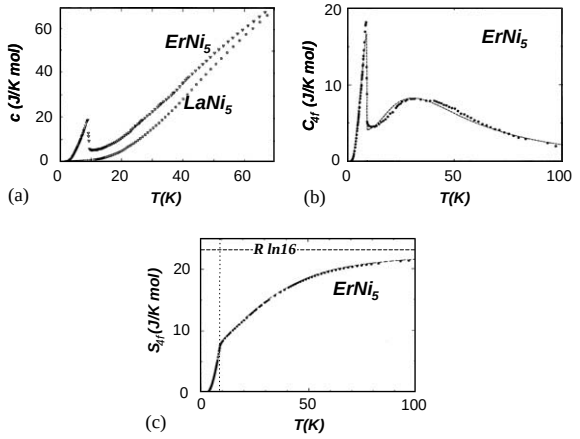

Fig. 6. Magnetic phase transition in $ErNi_5$. (a) Temperature dependence of the experimental heat capacity of single crystalline $ErNi_5$ and $LaNi_5$; (b) Temperature variation of the contribution of the f subsystem to the heat capacity of $ErNi_5$ derived as the difference of the molar specific heat of $ErNi_5$ and $LaNi_5$. The dotted line shows the f-subsystem contribution calculated for the atomic-like discrete energy spectrum determined by the strong spin–orbit coupling, CEF and spin–spin interactions; and (c) the temperature dependence of the experimental f-electron entropy, the calculations fully reproduce this dependence.

Systematic studies of the whole RNi_5 series [31,34,35] and other series [1] have provided strong experimental arguments for the high physical adequacy of the crystal-field theory to these intermetallic compounds. As main arguments we mention (i) the easy magnetic direction alternates with the sign of the α Stevens factor, (ii) the easy magnetic direction within the hexagonal plane alternates with the sign of the γ Stevens factor, (iii) the crystal-field coefficients are quite similar in the whole RNi_5 series [31,34], (iv) the description of many magnetic and electronic properties is very consistent, including the magnetic ordering.

We like to emphasize the good description of the specific heat at low temperatures, below 10 K in case of $ErNi_5$, in the presented CEF approach, complemented by inter-site magnetic interactions. In the CEF approach, excitations responsible for the low-temperature specific heat are the neutral, spin-like, not charge, excitations [36]. We think that charge excitations need too large energies to

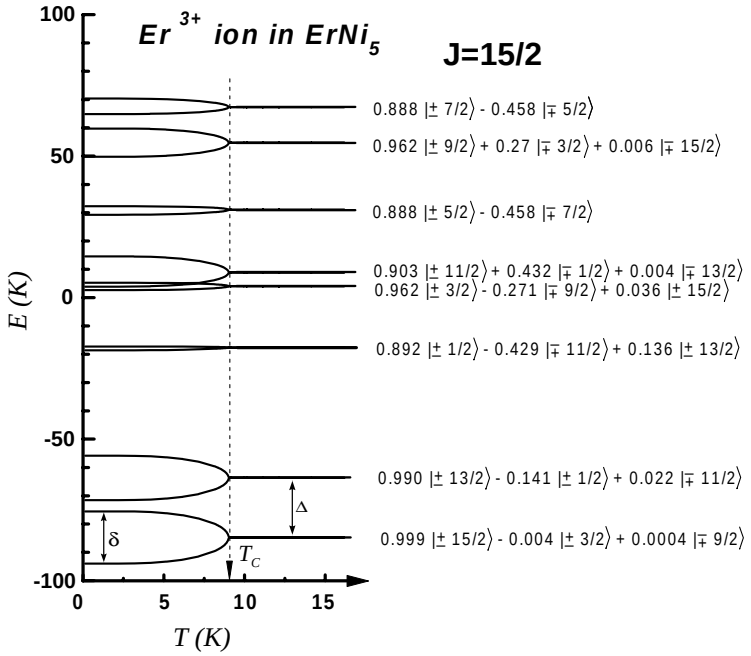

Fig. 7. Calculated electronic structure of the Er^{3+} ion in $ErNi_5$. Below 9 K, the magnetic state is formed which becomes visible by the splitting of the Kramers doublets.

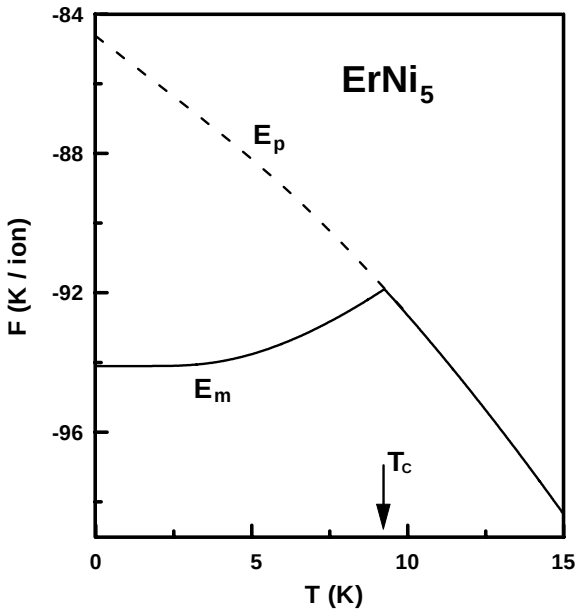

Fig. 8. Temperature dependence of the free energy for $ErNi_5$ in the paramagnetic (dashed line) and the ferromagnetic (solid line) state, showing the lower energy for the ferromagnetic state below T_c of 9.2 K.

take part in the low-temperature specific heat. One should also note that in the presented description of $c(T)$ there are somehow two contributions to the low-temperature specific heat: one related to excitations over a (small) gap to the Kramers-conjugate state, and other is related to the continuous increase of the ground-state energy due to magnetic interactions. This second effect mimics a gap-less low-temperature specific heat. By the formation of the magnetic state $ErNi_5$ gains the magnetic energy as is shown in Fig. 8.

7. $PrRu_2Si_2$ and $ErRu_2Si_2$

$PrRu_2Si_2$ and $ErRu_2Si_2$ crystallize in the tetragonal structure of the $ThCr_2Si_2$ type. They order ferromagnetically and antiferromagnetically below $T_c = 14$ K and $T_N = 6$ K, respectively. The magnetic ordering of both compounds is marked in the temperature dependence of the specific heat as a large λ anomaly. The experimentally observed ordered Er magnetic moment is $m_{Er} = 7.3\mu_B$ and

of the Pr-ions it is $2.7\mu_B$—thus in both cases 75% of the full trivalent moment. $PrRu_2Si_2$ exhibits uniaxial anisotropy along the tetragonal c-axis whereas $ErRu_2Si_2$ is a planar system with easy b-axis. $PrRu_2Si_2$ exhibits enormous magnetic anisotropy—the anisotropy field at 4.2 K is about 400 T. It corresponds to an MCA energy K_1 of 59 J/cm^3 [37] and largely exceeds the anisotropy of the $Nd_2F_{14}B$ supermagnet (of 12.5 J/cm^3). Unfortunately, this giant anisotropy is confined to low temperatures only which prohibits its technical application in the permanent-magnet industry.

The aim of the study of $PrRu_2Si_2$ and $ErRu_2Si_2$ was to find the origin of this giant MCA and the variation of the anisotropy from the Pr to the Er compound. Moreover, our interest for $PrRu_2Si_2$ was raised since its preceding compound, $CeRu_2Si_2$, exhibits pronounced heavy-fermion phenomena.

On the basis of all known magnetic and electronic properties of $PrRu_2Si_2$, we have attributed to the Pr^{3+} ions the configuration $4f^2$ and we constructed the energy level scheme of the Pr ion in $PrRu_2Si_2$. For the tetragonal symmetry CEF it contains five singlets and two doublets. The full set of CEF parameters is given by: $B_2^0 = -22$ K, $B_4^0 = +0.22$ K, $B_4^4 = +0.20$ K, $B_6^0 = -12$ mK and $B_6^4 = -45$ mK [38]. This set of CEF parameters describes well (i) the energy separations, revealed by inelastic neutron scattering [39], (ii) the anisotropic temperature dependence of the susceptibility in the paramagnetic region, (iii) the direction of the magnetic moment (along the tetragonal c-axis) in the ordered state, (iv) the spontaneous-moment value of the Pr ion at 4.5 K of $2.7\mu_B$, (v) the giant MCA of the magnetization curves at 4.5 K, and (vi) the temperature dependence of the specific heat with the λ-type peak at T_c.

The resulting energy-level scheme is shown in Fig. 9. It provides excitations observable in INS experiments at energies of 30 K ($\Gamma_{t1}^{(1)} \rightarrow \Gamma_{t2}$) and 330 K ($\Gamma_{t2} \rightarrow \Gamma_{t5}^{(1)}$ and $\Gamma_{t3} \rightarrow \Gamma_{t5}^{(1)}$, Γ_{t4}). These excitations have been observed in INS experiments by Mulders et al. [39] (2.25 and 29 meV). The derived electronic structure differs, however, from that derived in Ref. [39]—it has an extra state $\Gamma_{t3}^{(1)}$ at 58 K as second excited state. This state is invisible in the neutron-scattering studies due to small

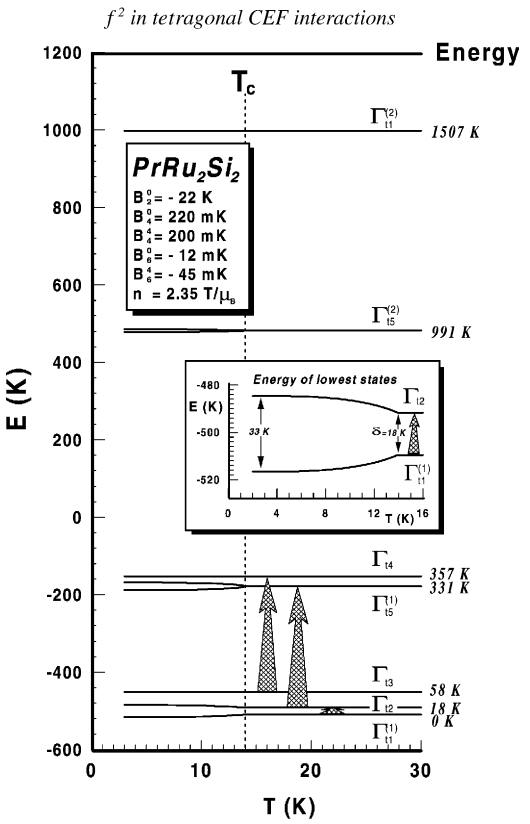

Fig. 9. Energy level scheme of the Pr^{3+} ion in $PrRu_2Si_2$. The tetragonal CEF interactions split the nine-fold degenerate ground-state multiplet $^3H_4$ into five singlets and two doublets. The three arrows indicate the allowed INS excitations. They are assigned to the ones experimentally detected in Ref. [39]. The inset shows details of the temperature variation of two lowest levels in the magnetic state.

matrix elements. We are quite convinced about the existence of a state at about 60 K as it largely improves the description of the temperature dependence of the specific heat.

It is interesting to note that the ordered state, with the large magnetic moment and the pronounced λ-peak is realized despite of the singlet ground state. The speciality of $PrRu_2Si_2$ is the electronic structure with two lowest singlets, $\Gamma_{t1}^{(1)}$ and Γ_{t2}, separated by 2 meV only—they form a two-level system that behaves as quasi doublet, see details of the energy levels shown in the inset of Fig. 9. This quasi-doublet behavior results from the large matrix element between these states. Thanks

to this, the magnetism of this system can be relatively easily induced by spin-dependent interactions despite of the generally non-magnetic character of singlets. One can say that such the quasi-doublet system is unstable with respect to magnetic instabilities. Such charge-formed ground state allows the appearance of the large magnetic moment of $2.7\mu_B$, in agreement with the experimental observation. The direction of the moment, along the c-axis, is related to the shape of the eigenfunctions of this two-level system. We would like to point out that the magnetic state in $PrRu_2Si_2$ with the singlet ground state is obtained in our calculations using the same computer program as used earlier for $ErNi_5$ and for $ErRu_2Si_2$, that have the Kramers-doublet ground state [40].

For the Er ion in $ErRu_2Si_2$, we derived a set of the tetragonal CEF parameters: $B_2^0 = +1.6\,K$, $B_4^0 = -5.0\,mK$, $B_4^4 = -4.5\,mK$, $B_6^0 = -5\mu K$ and $B_6^4 = -0.52\,mK$ [40], that is quite consistent with that found for $PrRu_2Si_2$ (direct single-ion recalculations of the $PrRu_2Si_2$ parameters give: $B_2^0 = +1.58\,K$, $B_4^0 = -4.97\,mK$, $B_4^4 = -4.52\,mK$, $B_6^0 = -105\,\mu K$ and $B_6^4 = -0.393\,mK$). The derived set of CEF parameters of $ErRu_2Si_2$ describes well: (i) the large anisotropy of the temperature dependence of the susceptibility in the paramagnetic region, (ii) the direction of the magnetic moment in the ordered state, (iii) the spontaneous moment of the Er ion of $m_{Er} = 7.2\mu_B$, (iv) the large anisotropy of the magnetization curves (with the substantial in-plane anisotropy), (v) the temperature dependence of the specific heat with the characteristic λ-type peak at T_N associated with the occurrence of the antiferromagnetic order, (vi) the tail of the Schottky-like peak above T_N, and (vii) the overall entropy.

At T_N of 6 K, the magnetic order starts to dominate the temperature disordering. In our calculations, this is accounted for by the effective parameter n_{RR} of $0.34\,T/\mu_B$ that yields B_{mol}^{Er} of 2.5 T at 0 K. The magnetic ordering produces an abrupt change in the energy level scheme, related to the removal of the Kramers degeneracy, that is manifested as the λ peak at T_N. The calculated moment of the Er ion, $7.2\mu_B$ at 0 K, consists of a spin and an orbital part ($m_s = +2.4\mu_B$ and $m_o = +4.8\mu_B$). The magnetic moment of the Er^{3+} ion is tied to the b direction within the tetragonal plane by the higher-order charge multipolar interactions.

The consistent description of so many physical properties of so different compounds as $PrRu_2Si_2$ and $ErRu_2Si_2$, containing ions with non-Kramers and Kramers electron system, provides strong support for the presented theoretical approach. It confirms the existence of the discrete atomic-like electronic structure in intermetallic compounds. These studies confirm the importance of low-symmetry charge multipolar interactions and the essential need for taking into account all CEF terms, including higher-order terms, in the description of the magnetic properties of 4f systems.

In the description of rare-earth atoms in compounds we employ the J quantum number for the description of the magnetism and the electronic structure. In this approximation, the spin–orbit coupling is taken as infinitively strong, $\lambda_{s-o} = \infty$. We checked how taking into account a finite value of λ_{s-o} corrects the results by making calculations in the spin–orbit LS space for the $4f^1$ system, i.e. for the Ce^{3+} ion. It turns out, that taking into account a realistic value of the spin–orbit coupling of 1000 K does not lead to any essential changes in the magnetism and in the electronic structure associated with the lowest multiplet. Of course, the finite value of λ_{s-o} puts the excited multiplet at an energy of about 2500 K, as it is detected experimentally. The most important is the fact that the expectation values of L_z and S_z of the ground state of the Ce^{3+} ion are practically the same as derived in calculations by means of the J, J_z functions [40]. This means that, though calculations for rare-earth atoms should be made within the $|LSL_zS_z\rangle$ space, much simpler calculations within the $|LSJJ_z\rangle$ space provide practically the same results. This conclusion is, of course, not valid for 3d atoms, where there is a need for calculations within the $|LSL_zS_z\rangle$ space owing to the weaker spin–orbit coupling [41].

8. Conclusions

We have presented a microscopic description of the magnetic and electronic properties for different

compounds containing an open 4f-shell atom, like Ho_2Co_{17}, $Nd_2Fe_{14}B$, $Pr_2Fe_{14}B$, $ErNi_5$, $PrRu_2Si_2$, $NdRu_2Si_2$, performed within the same crystal-field model, complemented by inter-site magnetic interactions. It reveals the existence in a solid of discrete low-energy states originating from the highly correlated atomic-like electron system $4f^n$. Strong correlations among f electrons we take into account by two Hund's rules. The low-energy scale is of about 25 meV and lower which causes its importance for solid-state physics, including the description of magnetic and electronic properties at, room temperature and lower. We take into account the intra-atomic spin–orbit coupling and crystal-field interactions. By pointing out the importance of crystal-field interactions, we understand that CEF interactions have to be considered for all transition-metal compounds containing open-shell atoms at the beginning of any analysis of their magnetic and electronic properties. The crystal-field theory points out the importance of lattice distortions and the local symmetry on atomic scale and discusses a solid in real space. Thanks to this, the presented approach can be applied to systems with the broken translational symmetry.

The formation of the magnetic state can be traced on the atomic scale. At the magnetic ordering temperature the time-reversal symmetry is broken which is visible in the eigenfunctions and in the splitting of Kramers-doublet states. By the magnetic ordering the system gains magnetic energy. The presented approach is remarkably successful. It shows its high physical adequacy despite of serious objections that the CEF-based model cannot be applied to intermetallics. Our single-ion CEF origin, for instance, of the MCA in Ho_2Co_{17} was opposed at the beginning by other mechanisms like anisotropic exchange. Moreover, the applicability of the CEF theory and the existence of the discrete CEF states in an intermetallic compound was seriously questioned. These other approaches at present somehow have disappeared but the CEF model seems to have survived.

The application of the presented approach to 3d- and 5f-open shell compounds is quite promising [41,42]. The good description of experimental results indicates the existence of the discrete atomic-like states in 3d/4f/5f systems in the meV energy scale. This low-energy atomic-like electronic structure predominantly determines electronic and magnetic properties.

References

[1] J.J.M. Franse, R.J. Radwanski, in: K.H.J. Buschow (Ed.), Handbook of Ferromagnetic Materials, Vol. 7, North-Holland, Amsterdam, 1993, p. 307.
[2] J.J.M. Franse, F.R. de Boer, P.H. Frings, R. Gersdorf, A. Menovsky, F.A. Muller, R.J. Radwanski, S. Sinnema, Phys. Rev. B 31 (1985) 4347.
[3] R. Verhoef, R.J. Radwanski, J.J.M. Franse, J. Magn. Magn. Mater. 89 (1990) 176.
[4] R.J. Radwanski, J.J.M. Franse, J. Magn. Magn. Mater. 46 (1985) 289.
[5] R.J. Radwanski, J.J.M. Franse, Physica B 154 (1989) 181.
[6] R.J. Radwanski, J.J.M. Franse, S. Sinnema, J. Phys. F 15 (1985) 969.
[7] R.J. Radwanski, J.J.M. Franse, Acta Phys. Pol. A 68 (1985) 401.
[8] R.J. Radwanski, J.J.M. Franse, S. Sinnema, J. Magn. Magn. Mater. 51 (1985) 175.
[9] F. Tomiyama, M. Ono, M. Date, A. Yamagishi, R. Verhoef, F.R. de Boer, J.J.M. Franse, X.P. Zhong, J. Appl. Phys. 69 (1991) 5539.
[10] S. Sinnema, J.J.M. Franse, A. Menovsky, R.J. Radwanski, J. Magn. Magn. Mater. 54–57 (1986) 1639.
[11] R.J. Radwanski, X.P. Zhong, F.R. de Boer, F.M. Yang, J.Y. Li, T. Kohashi, M. Ono, M. Date, A. Yamagishi, J. Magn. Magn. Mater. 104–107 (1992) 1139.
[12] R.J. Radwanski, J.J.M. Franse, Phys. Rev. B 36 (1987) 8616.
[13] R.J. Radwanski, Physica B 142 (1986) 57.
[14] R.J. Radwanski, J.J.M. Franse, P.H. Quang, F.E. Kayzel, J. Magn. Magn. Mater. 104–107 (1992) 1321.
[15] R. Ballou, R.J. Radwanski, R. Lemaire, J.J.M. Franse, Physica B 177 (1992) 193.
[16] R.J. Radwanski, Phys. Stat. Sol. B 137 (1986) 487.
[17] R.J. Radwanski, Z. Phys. B 65 (1986) 65.
[18] J.H.P. Colpa, S. Sinnema, P.H. Frings, J.J.M. Franse, R.J. Radwanski, J. Phys.: Condens. Matter 1 (1989) 2047.
[19] J.H.P. Colpa, P.H. Frings, R.J. Radwanski, J.J.M. Franse, M. Alba, J. Magn. Magn. Mater. 131 (1994) 167.
[20] R.J. Radwanski, J.J.M. Franse, R. Verhoef, J. Magn. Magn. Mater. 83 (1990) 127.
[21] T.H. Jacobs, K.H.J. Buschow, G.F. Zhou, J.P. Liu, X. Li, F.R. de Boer, J. Magn. Magn. Mater. 104–107 (1992) 1275.
[22] F.R. de Boer, X.P. Zhong, K.H.J. Buschow, T.H. Jacobs, J. Magn. Magn. Mater. 90 & 91 (1990) 25.

[23] J.P. Liu, F.R. de Boer, P.F. de Châtel, R. Coehoorn, K.H.J. Buschow, J. Magn. Magn. Mater. 132 (1994) 159.
[24] M. Sagawa, S. Fujimura, M. Togawa, H. Yamamoto, Y. Matsuura, J. Appl. Phys. 55 (1984) 2083;
J. Herbst, J. Croat, F.E. Pinkerton, W. Yellon, Phys. Rev. B 29 (1984) 4176.
[25] S. Sinnema, R.J. Radwanski, J.J.M. Franse, D.B. de Mooij, K.H.J. Buschow, J. Magn. Magn. Mater. 44 (1984) 333.
[26] R. Verhoef, J.J.M. Franse, A.A. Menovsky, R.J. Radwanski, Ji Song-Quan, Yang Fu-Ming, H.S. Li, J.P. Gavigan, J. Phys. 49 (1988) C8-565.
[27] R.J. Radwanski, J.J.M. Franse, J. Magn. Magn. Mater. 80 (1989) 14.
[28] R.J. Radwanski, R. Verhoef, J.J.M. Franse, J. Magn. Magn. Mater. 83 (1990) 141.
[29] R.J. Radwanski, J.J.M. Franse, Acta Phys. Pol. A 90 (1996) 223.
[30] J.J.M. Franse, R.J. Radwanski, in: J.M.D. Coey (Ed.), Rare-earth Iron Permanent Magnets, Oxford, 1996, pp. 58–158.
[31] R.J. Radwanski, N.H. Kim-Ngan, F.E. Kayzel, J.J.M. Franse, D. Gignoux, D. Schmitt, F.Y. Zhang, J. Phys.: Condens. Matter 4 (1992) 8853.
[32] R.J. Radwanski, J.J.M. Franse, D. Gignoux, F.E. Kayzel, C. Marquina, A. Szewczyk, Physica B 177 (1992) 291.
[33] F. Kayzel, J.J.M. Franse, R.J. Radwanski, IEEE Trans. Magn. 30 (1994) 1087.
[34] F.Y. Zhang, D. Gignoux, D. Schmitt, J.J.M. Franse, F.E. Kayzel, N.H. Kim-Ngan, R.J. Radwanski, J. Magn. Magn. Mater. 130 (1994) 108.
[35] R.J. Radwanski, Z. Ropka, R. Michalski, in: M. Donath, P.A. Dowben, W. Nolting (Eds.), Magnetism and Electronic Correlations in Local-Moment Systems, World Scientific, Singapore, 1998, p. 445.
[36] R.J. Radwanski, Solid State Commun. 99 (1996) 981.
[37] R. Michalski, Z. Ropka, R.J. Radwanski, Acta Phys. Pol. A 97 (2000) 767.
[38] R. Michalski, Z. Ropka, R.J. Radwanski, J. Phys.: Condens. Matter 12 (2000) 7609.
[39] A.M. Mulders, A. Yaouanc, P. Dalmas de Reotier, P.C.M. Gubbens, A.A. Molenaar, B. Fak, E. Ressouche, K. Prokes, A.A. Menovsky, K.H.J. Buschow, Phys. Rev. B 56 (1997) 8752.
[40] R. Michalski, Thesis, University of Mining and Metallurgy, Krakow 2001, available on http://www.css-physics.edu.pl.
[41] Z. Ropka, R. Michalski, R.J. Radwanski, Phys. Rev. B 63 (2001) 172404.
[42] R.J. Radwanski, R. Michalski, Z. Ropka, Acta Phys. Pol. B 31 (2000) 3079.